


Article

Dielectric Property and Space Charge Behavior of Polyimide/Silicon Nitride Nanocomposite Films

Minghua Chen *, Wenqi Zhou, Jiawei Zhang and Qingguo Chen *

Key Laboratory of Engineering Dielectric and Applications (Ministry of Education), Harbin University of Science and Technology, Harbin 150080, China; zhouwenqi0827@163.com (W.Z.); jwzhang@hrbust.edu.cn (J.Z.)

* Correspondence: mhchen@hrbust.edu.cn (M.C.); qgchen@263.net (Q.C.)

Received: 16 December 2019; Accepted: 27 January 2020; Published: 4 February 2020



Abstract: Polymeric materials have many applications in multiple industries. In this paper, silicon nitride nanoparticles (Si_3N_4) were incorporated into a polyimide (PI) matrix to obtain composite films via the in situ polymerization method. The Si_3N_4 nanoparticles were consistently scattered in the composites, and the thickness of PI/ Si_3N_4 films was around 50 μm . The effects of nanoparticle content on the dielectric constant, loss tangent and breakdown strength were simultaneously studied. A 3 wt.% doped PI/ Si_3N_4 film revealed excellent dielectric properties, a dielectric constant (ϵ) of 3.62, a dielectric loss tangent ($\tan\delta$) of 0.038, and a breakdown strength of 237.42 MV/m. The addition of Si_3N_4 formed an interface layer inside PI, resulting in a large amount of space charge polarization in the electric field. The space charge of materials from the microscopic point of view was analyzed. The results show that there are trapenergy levels in the composites, which can be used as a composite carrier center and transport channel, effectively improving the performance of a small amount of nanoparticles film.

Keywords: polyimide; silicon nitride; dielectric properties; space charge

1. Introduction

Polyimide (PI) has been broadly used in the fields of electronic packing, the automotive and chemical industries, aerospace and precision machinery, etc. [1–3] due to its low dielectric constants, outstanding mechanical properties, high resistance to various temperatures (400 °C), excellent solvent resistance and good biocompatibility [4]. Furthermore, recent downsizing of current and cost reduction demands a reduction in its thickness. This means that the polyimide film is required to show a good performance as an insulating material under a high electric field and to keep the dielectric constant in some level.

In order to achieve this goal, there have been great efforts to use high dielectric constant fillers, such as linear, flaky carbon materials or metal materials. In the literature, a lot of composite systems have been investigated, including different kinds of fillers (SiC [5], ZnO [6], AG [7], MWCNTs [8], Ni [9], CNTs and graphene oxide [10]), indicating that dropping nanofillers can effectively upraise dielectric constant. However, carbon and metal materials have high electrical conductivity, which seriously affects the insulating properties of the polymer, resulting in a dilemma that the dielectric strength and dielectric constant can only be improved.

To maintain a distance from this shortcoming, researchers have proposed that the ceramic materials ($\text{Ba}_{0.5}\text{Sr}_{0.5}\text{TiO}_3$ [11], BaTiO_3 [12,13]) would be excellent candidates for inorganic fillers. Among such a significant number of materials, silicon nitride (Si_3N_4) has attracted significant consideration owing to its captivating properties, such as wide band gap, excellent insulation performance, high quality at high temperature, and fantastic thermal conductivity [14]. Diahm et al. argued that the epoxy/ Si_3N_4 (1 vol.%) nanocomposites show an improvement of the dielectric strength, by about

1.16 times, compared to pure epoxy [15]. Xu et al. obtained the polypropylene/Si₃N₄ (2 wt.%) and indicated that breakdown strength was increased by about 1.1 times [16]. He et al. suggested that the polystyrene/Si₃N₄ (40 vol.%) can increase the dielectric constant from 2.4 to 3.5 [17]. Yan et al. proposed that the Si₃N₄/epoxidized silane/cyanate ester can enhance the dielectric constant from 2.93 to 3.03 in 10 MHz [18]. Zhou et al. detailed that the polyethylene/Si₃N₄ (20 wt.%) increased the dielectric constant by about two times [19]. Previous research seems to be able to meet the requirements, which have increased the dielectric strength and dielectric constant of organic polymers by the doping of silicon nitride. Most of these works focused on dielectric and thermal properties, with less attention to the breakdown mechanism. There is still a lack of effective models and deep explanations for the mechanism of breakdown strength [20].

In this paper, we report an in situ polymerization process to prepare PI/Si₃N₄ nanocomposite films. The Si₃N₄ nanoparticles were consistently scattered in the composites, and the thickness of the PI/Si₃N₄ films was around 50 μm. Their electrical conductivity space charge distribution and thermal stability were studied systematically. An innovative attempt was made to explain the mechanism of breakdown by space charge. The PI/Si₃N₄ film with 3 wt.% Si₃N₄ substance introduced an exceptional heat resistance index of 279 °C, an excellent dielectric performance (ϵ and $\tan\delta$ respectively from 3.3 to 3.2 and 0.0032 to 0.0112 at frequency range of 10² to 10⁶ Hz), and a dielectric strength of 237.42 MV/m.

2. Experimental

2.1. Materials

Both 4,4'-diaminodiphenylether (ODA) and 1,2,4,5-benzenetetracarboxylic anhydride (PMDA) were acquired from Sinopharm Chemical Reagent Co., Ltd., Shanghai, China. *N,N*-dimethylacetamide (DMAC) was gotten from Tianjin in Fuyu Fine Chemical Co., Ltd., Tianjin, China. Silicon Nitride (Si₃N₄) was acquired from Shanghai Macklin Biochemical Co., Ltd., Shanghai, China, with a density of 3.44 g/mL and a particle size between 10 and 30 nm.

2.2. Preparation

The films were prepared by a two-step method with various loadings of Si₃N₄. The schematic chart that addresses the readiness of PI/Si₃N₄ composites is displayed in Figure 1a.

Firstly, we synthesized the poly(amide acid) (PAA) and PAA/Si₃N₄ precursors slurry. Initially, a certain amount of Si₃N₄ was scattered in 36 mL DMAC by sonication for a certain time. Along with DMAC, ODA (3 g, 0.013 mol) was added to a 250 mL three-necked flask outfitted with a mechanical stirrer. After the diamines were broken up, equimolar PMDA (3.28 g, 0.013 mol) was added in one portion to the flask. Consequently, the homogeneous viscous pulp of PAA (precursor of polyimide) and PAA/Si₃N₄ was obtained. Finally, this solution was cast on a glass substrate by a scraper blade. The second step was the thermal imidization process. To remove the residual solvent of DMAC, the film was placed in a vacuum oven at 80 °C for 4 h. After that, the composite was further thermally treated in a muffle furnace by the gradient heating method, from room temperature to 110, 140, 170, 200, 230, 260, 290, 320, and 350 °C for half an hour, then the PAA was changed over to PI totally. The PI and PI/Si₃N₄ nanocomposites (PI, PI/Si₃N₄-1, PI/Si₃N₄-3, PI/Si₃N₄-5 and PI/Si₃N₄-7) containing 0, 1, 3, 5 and 7 wt.% of Si₃N₄ were set up by the previously mentioned experimental processes.

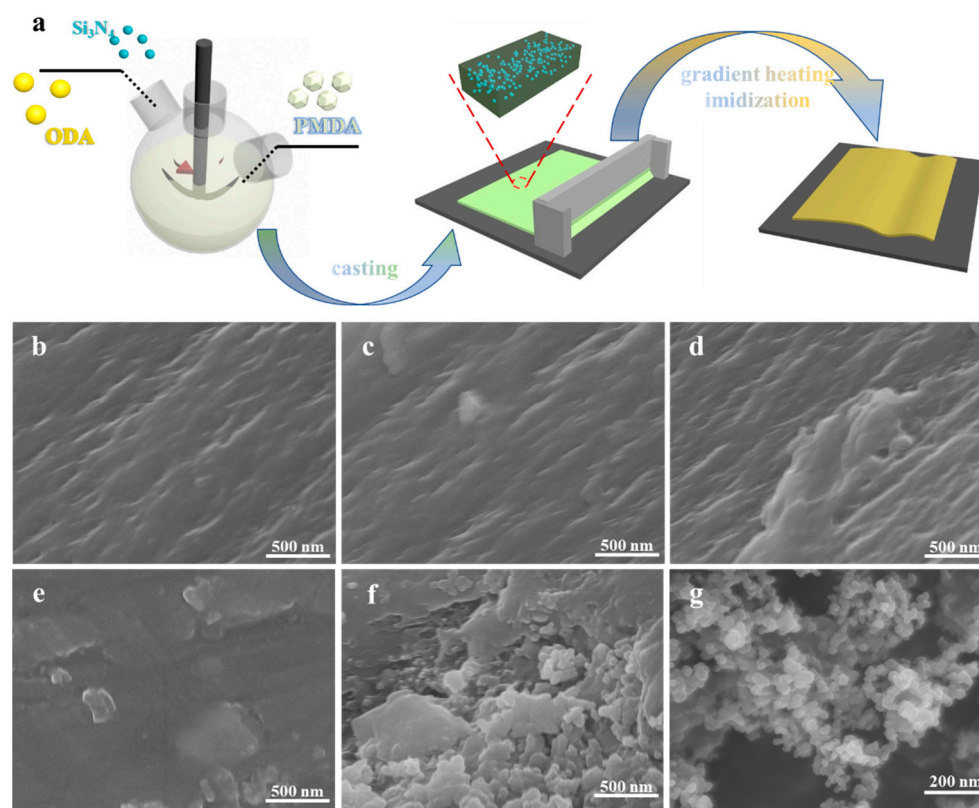


Figure 1. Preparation process of the PI/Si₃N₄ composites (a). SEM images of the cross-section of the pure polyimide (PI) (b), the 1 wt.% PI/Si₃N₄ (c), the 3 wt.% PI/Si₃N₄ (d), the 5 wt.% PI/Si₃N₄ (e), and the 7 wt.% PI/Si₃N₄ (f) nanocomposite films, and pure Si₃N₄ powder (g).

2.3. Characterization

The microstructures of the composite films were taken on a SU8020 scanning electron microscope (SEM, Hitachi, Tokyo, Japan). Before testing, all the sample fracture surfaces were brittle broken by liquid nitrogen and coated with gold. Fourier transform infrared (FTIR) spectra were obtained on Perkin Elmer's Spectrum Two L160000A, PerkinElmer, Waltham, MA, USA.

The dielectric constant (ϵ) and dielectric loss factor ($\tan\delta$) values of the samples (25 mm \times 25 mm) were measured using Concept 80 at frequencies ranging from 10 to 10^6 Hz. The samples were fabricated by sputtering a thin film aluminum pattern on both sides. The electric breakdown strength was measured using the HT-5/20A equipment with a 1 kV/s loading rate of voltage and the area of the copper electrode used was 3.14 cm² at room temperature. The space charge distribution measurement of the specimen with an average thickness of 100 μ m was performed in a pulse electro-acoustic (PEA) system. Silicone oil was used as acoustic coupling to ensure sound acoustic transmission between the specimen and the electrode. Calibration was conducted at a DC field of 3 kV/mm for 5 min to minimize the influence on space charge accumulation. Then, a DC electric field of 40 kV/mm was applied to the specimen for 30 min at room temperature and removed. The measurement signals, both in the polarization and depolarization process, were recorded over time, and the data were processed using a calibration trace and a deconvolution technique to restore the original signal. The thermogravimetric analysis (TGA) measurements were carried out using Pyris6 from 50 to 800 $^{\circ}$ C in the air at a heating rate of 10 $^{\circ}$ C/min.

3. Results and Discussion

3.1. Structure Characterization of PI/Si₃N₄

Figure 1b–f separately shows the fracture morphologies of PI/Si₃N₄ composites with different Si₃N₄ mass contents from 1 to 7 wt.%. When the doping amount is meager, the dopants are evenly distributed in the polymer, and they are far away from each other. With the increasing of the dopant, the distance between the nanoparticles became closer and closer. Thus, the fracture morphologies of the PI/Si₃N₄ composites were much rougher.

When the filler aggregated to a certain extent, the gap was almost gone, as depicted in Figure 1f. In addition, the disappearance of the gap leads to the formation of a conductive path and damages the insulation performance. This poor dispersion in high filler content was mainly attributed to the van der Waals force and the inevitable interfacial thermal barriers between fillers and the PI matrix.

The FTIR spectra of pure Si₃N₄ nanoparticles and PI/Si₃N₄ matrix are presented in Figure 2a. The absorption bands near 1650 cm⁻¹ (amic acid C=O stretching) and 1550 cm⁻¹ (amide C–N stretching) in PI/Si₃N₄ matrix are both disappeared, which proves that the thermal imidization of PAA is completed [21]. The bands near 1778 cm⁻¹ and 1726 cm⁻¹ can be ascribed to the asymmetrical and symmetrical stretching vibration of the C=O groups, respectively [22]. The characteristic stretching vibration peak at 1379 and 1116 cm⁻¹ can be assigned to the C–N group, and the bending vibration peak at 720 cm⁻¹ can be attributed to the imide group [23]. In addition, all the FTIR curves of the PI/Si₃N₄ complexes present clear characteristic absorption peaks near 3533, 1647, 1074, 952 and 447 cm⁻¹, owing to the incorporation of Si₃N₄ nanoparticles [24,25].

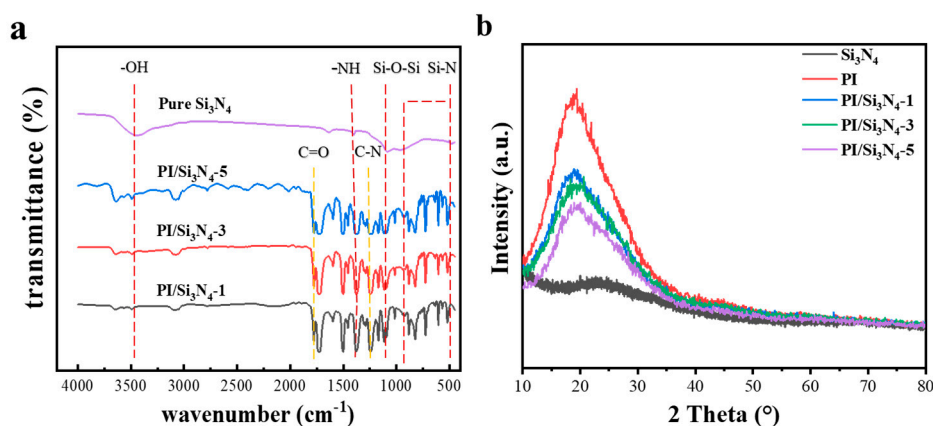


Figure 2. FTIR (a) and XRD (b) spectra of pure Si₃N₄ nanoparticles and PI/Si₃N₄ matrix.

As can be seen in Figure 2b, similar curves were observed for all the samples. It can be clearly seen that there is no special peak in silicon nitride, indicating that it is amorphous [16]. The diffraction peak at about 20° of PI decreased progressively with the addition of nano-silicon nitride, which demonstrated that nanoparticles had been successfully combined.

3.2. Thermal Properties of PI/Si₃N₄

As can be seen from Figure 3 and Table 1, when the temperature is above 550 °C, the polymer begins to degrade rapidly, and the maximum degradation rate is around 600 °C. At the same time, the corresponding heat resistance index of pure PI and PI/Si₃N₄ composites are 259 °C, 272 °C (1 wt.%), 279 °C (3 wt.%), 279 °C (5 wt.%), 279 °C (7 wt.%), respectively. The results show that the thermal stability of the composites is improved, which is due to the high thermal conductivity of silicon nitride.

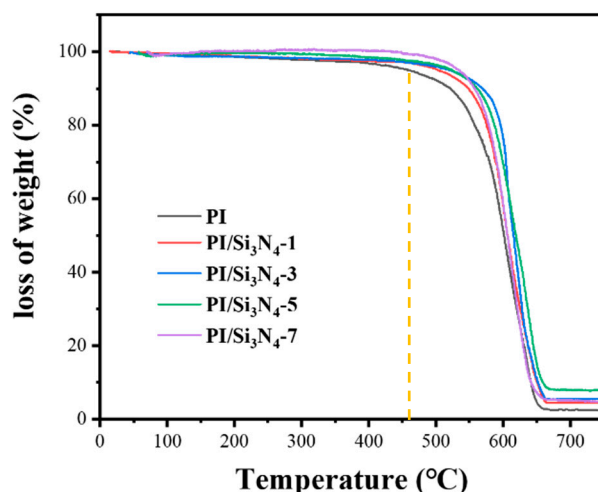


Figure 3. TGA analysis of PI and PI/Si₃N₄ films.

Table 1. Characteristic thermal data of PI and PI/Si₃N₄ composites.

Samples	Weight Loss Temperature (°C)		$T_{\text{heat-resistance index 1}}$ (°C)	T_{max} (°C)
	5%	30%		
PI	454.6	577.8	258.9748	607.3
PI/Si ₃ N ₄ -1	502.5	589.5	271.803	611.6
PI/Si ₃ N ₄ -3	519.4	603.2	279.1432	613.4
PI/Si ₃ N ₄ -5	524.4	599.3	278.9766	637.1
PI/Si ₃ N ₄ -7	538.8	590.2	279.1236	625.4

¹ $T_{\text{heat-resistance index}} = 0.49 \times [T_5 + 0.6 \times (T_{30} - T_5)]$, T_5 , T_{30} is the decomposing temperature at 5%, 30% weight loss, respectively.

3.3. Electrical Properties of PI/Si₃N₄

Figure 4a demonstrates that both the dielectric constant (ϵ) and dielectric loss tangent ($\tan\delta$) were upgraded after dropping. The PI/Si₃N₄-7wt.% hybrid film exhibits a maximum dielectric constant of 3.62 at 100 Hz. More surprisingly, the dielectric loss tangent remains at a low level ($\tan\delta = 0.0038$). The quantity of orientation polarization groups for the PI/Si₃N₄ composites were increased step by step with the expanding mass fraction of Si₃N₄ fillers, beneficial to the improvement of the ϵ value. Furthermore, the dielectric loss tangent increased at the range of 10^5 to 10^6 Hz, which can be credited to the dielectric relaxation behaviors of polyimide. Dielectric loss alluded to the phenomenon that dielectric composites converted electrical energy into heat energy when subjected to an alternating electric field. It is worth noting that the dielectric loss of the complex shows almost no difference in low frequencies, and the value of PI/Si₃N₄-3 wt.% is especially outstanding. According to the micro capacitance theory [26], this phenomenon is mainly because the micro capacitance increases when the dopant content increases, leading to more significant dielectric loss. Due to the action of the external electric field, the dipole molecules in the medium repeatedly arrange and rub against each other as the frequency increases, resulting in polarization loss. The higher the dipole moment is, the higher the dielectric loss is.

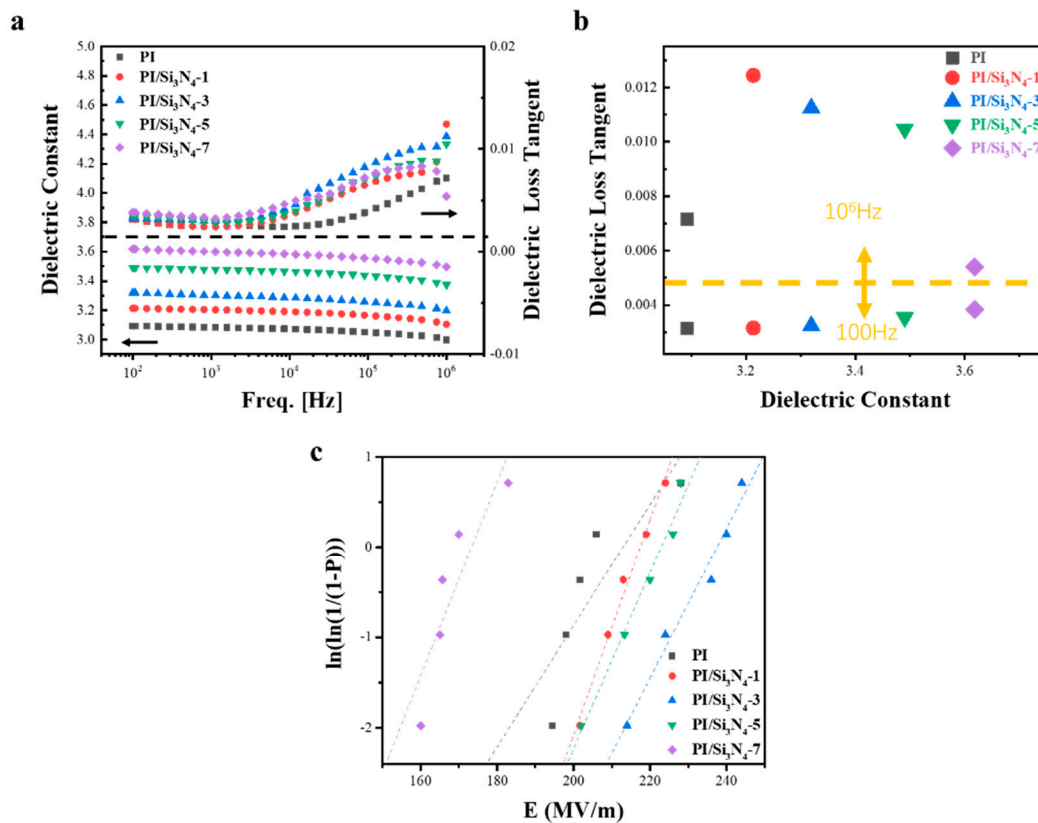


Figure 4. The mass fraction of Si₃N₄ fillers affecting (a) the dielectric constant (ϵ) and dielectric loss tangent ($\tan\delta$) values at a different frequency; (b) between dielectric constant (ϵ) and dielectric loss tangent ($\tan\delta$) values at 100 and 10⁶ Hz of the PI/Si₃N₄ composites; and (c) Weibull-distribution plot of breakdown strength for PI/Si₃N₄ composites.

The dielectric constant and dielectric strength of dielectric materials jointly determine their maximum stored energy, and the relationship of these three factors is shown in the following equation:

$$U_e = \frac{1}{2} \epsilon_0 \epsilon E_b^2$$

where U_e is the discharged energy density, ϵ_0 is the vacuum dielectric constant ($\epsilon_0 = 8.85 \times 10^{-12}$ F m⁻¹), ϵ is the dielectric constant of the composite, and E_b is the breakdown strength of the complex. Since E_b is a quadratic independent variable, it has a greater impact on energy storage. Therefore, it is an effective way to improve the energy storage performance of materials to keep the dielectric constant constant or even increase while increasing the dielectric strength. We analyzed the strength of pure PI and composite films by using the two-parameter Weibull distribution function:

$$P = 1 - \exp\left[-\left(\frac{E_b}{\alpha}\right)^\beta\right]$$

where P is the cumulative probability of electric failure, E_b is the measured breakdown field, scale parameter α is the breakdown strength, for which there is a 63.2% probability for the sample to breakdown (Weibull E_0), and shape parameter β is associated with the scattering of the data distribution. Let us take the logarithm of both sides of this equation:

$$\ln[-\ln(1 - P)] = \beta(\ln E_b - \ln \alpha)$$

In addition, for each measured value, the P is determined according to the following formula:

$$P = \frac{i - 0.44}{n + 0.25}$$

where i is the descending rank of the E value in the total breakdown sample data, and n is the total number of sample spaces [27].

In Table 2, all the PI/Si₃N₄ films have high β values, indicating that these composites were of a high quality and dependability. The breakdown strengths of these composites with various concentrations are plotted in Figure 4c. It is obvious that the breakdown strength of PI/Si₃N₄-3 wt.% is 237.42 MV/m, 1.12 times higher than pure PI (212.42 MV/m). This is mainly because the ceramic filler itself exhibits high insulation, and the clustering phenomenon was not evident when the doping degree was lower than 7 wt.% (173.05 MV/m). The polyimide matrix with uneven packing distribution cannot evenly wrap Si₃N₄, resulting in defects and voids in the film, causing a distorted electric field distribution. As a result, the PI/Si₃N₄-7 wt.% composites will be divided into multilayers, which are conducive to develop breakdown strengths under the electric field. We can also see the correlation coefficients R in Table 2, which are all closer to 1, meaning that the analysis data for breakdown has a suitable fitting [28].

Table 2. Linear fitting results and Weibull parameters of PI composite films.

Samples	Linear Fitting Results			Weibull Parameters	
	Slope	ln[-ln(1-P)] Intercept	R	β	E ₀
PI	14.392	-77.122	0.75	14.392	212.42
PI/Si ₃ N ₄ -1	25.346	-136.4	0.99	25.346	217.36
PI/Si ₃ N ₄ -3	18.91	-103.43	0.97	18.91	237.42
PI/Si ₃ N ₄ -5	20.871	-112.84	0.98	20.871	222.84
PI/Si ₃ N ₄ -7	18.601	-95.86	0.82	18.601	173.05

According to the intrinsic theory [29], the electric field will cause the breakdown of a material in a very short time, without the effects of high field aging. Under the action of the external electric field, there may be some electrons in the conduction band of the solid, and these electrons will gain energy movement due to the action of the external electric field, and the movement will interact with the lattice wave (phonons). When the energy gained by the electrons is much higher than the energy required to interact with lattice waves, their interaction will ionize new electrons, free electrons will increase, and then the breakdown phenomenon occurs.

Due to the influence of the end group and impurity, the molecular structure will not be exactly ideal, and the electrons will not to be appear in pairs. As illustrated in Figure 5, when the external electric field acts, electrons that do not form covalent bonds will gain energy and become free electrons, which will move in the polymer along with the direction of the electric field. The free electrons have a certain probability of being captured by various elements, like Si, bringing about the breaking of the covalent bond and the appearance of extra electrons at the other end of the element, as N. What is more, on the grounds that the electric field is offering energy to these extra electrons, these atoms are going to snatch electrons from other atoms, such as O, shaping new covalent bonds. As the external electric field is strong enough, the energy of the excess electrons becomes larger and larger, and instead of forming covalent bonds, they bombard the molecular chain, causing ionization to produce secondary electrons and leading to electron collapse. Similarly, at the same field strength, when the dopant reaches a certain level, the polymer cannot adequately wrap the dopant, and will generate more excess electrons, which is more likely to cause electron collapse [30].

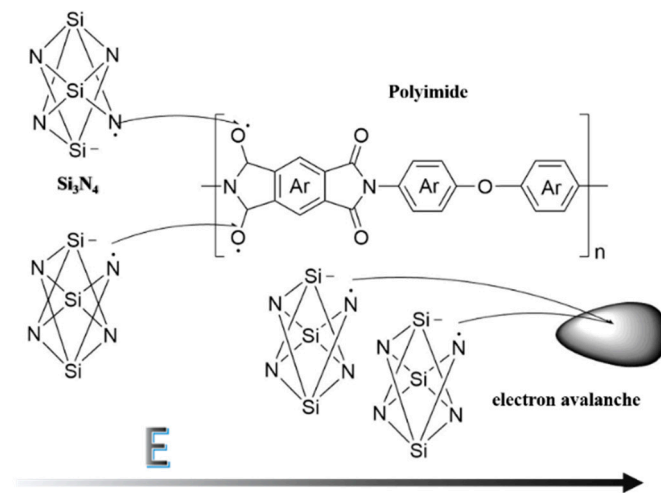


Figure 5. The model of electron avalanche for PI/Si₃N₄.

From the above inference, it is well known that the primary driver of a breakdown caused by electron collapse in the medium is the amassing of charge. Therefore, in order to understand the space charge characteristics of the complex, we selected the pure PI, the 3 wt.% PI/Si₃N₄, the 5 wt.% PI/Si₃N₄, and the 7 wt.% PI/Si₃N₄ nanocomposite films for space charge measurement (Figure 6). If the positive and negative charges in each repeating element in a homogeneous dielectric cannot counteract each other, the excess charge is the space charge at that position. In this paper, the space charge mainly refers to the trapped charge and the polarization charge caused by non-uniform polarization.

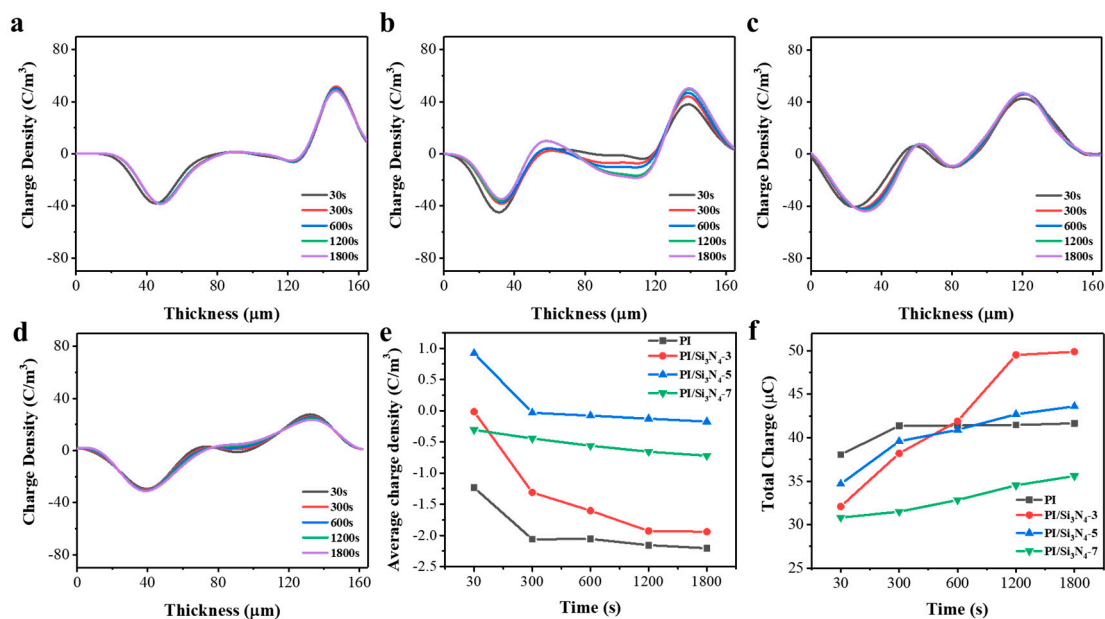


Figure 6. Space charge distribution in the pure PI (a), the 3 wt.% PI/Si₃N₄ (b), the 5 wt.% PI/Si₃N₄ (c) and the 7 wt.% PI/Si₃N₄ (d) nanocomposite films, and the curves of the average charge density of these (e) and the total charge quantity of these (f).

As can be seen from Figure 6a, for pure polyimide films, the space charge is mainly distributed on the surface near the electrode, and the internal charge accumulation is almost zero. However, it is evident that a hetero-charge appears in the vicinity of electrodes (Figure 6b–d) in the composites.

It can be seen from Figure 6e, with the time of applied electrical field increasing, the negative charge is obviously accumulated. However, the doping of Si₃N₄ reduces the negative space charge

generated by the medium when the electric field is first applied, providing a positive space charge. At 3 wt.% doping, the positive and negative charges almost completely neutralize each other when the electric field is applied for 30 s. With the increase in applied time, the trend is basically the same as that of the undoped film. When the doped content is 5 wt.%, the positive charge accumulates for the most part at 30 s of the electrical field being applied. With the applied time increase, the positive and negative charges almost completely cancel out, thus the change is not obvious, and the average positive and negative charge density remains around 0. When the doped content is 7 wt.%, the change in the average charge density does not show a linear function relationship, and the change range is the least.

As can be seen from Figure 6f, the total charge of the undoped pure film is the most when the electric field is applied for 30 s, and the total charge does not change after the electric field is applied for 300 s. The 3 wt.% doped film rapidly accumulates charge before applying the electric field for 1200 s. Combined with Figure 6e, it can be seen that the negative charges are rapidly accumulating, and no charge accumulates from 1200 s to 1800 s. The 5 wt.% doped film accumulates space charge from 30 s to 1800 s, only the accumulation rate is slower than 3 wt.% doping. The 7 wt.% doped and 5 wt.% doped film accumulation process is similar, but the speed is slower. This phenomenon can be attributed to the trap effect of the medium.

As Tanaka supposed [31], a multi-core model of the interface of a spherical inorganic filler nanoparticles doped in polyimide is shown in Figure 7a. The first layer is a bonded layer, which consists of combined filler and polyimide matrix by ionic, covalent or hydrogen bonds. The second layer is a bound layer dependent on the van der Waals force and is the main layer of polymer conformation. These two layers present deep traps. The third layer is considered to be a region affected chemically by the second layer, and electrically by the diffuse Gouy–Chapman layer to form a somewhat amorphous morphology, and is the main source of shallow traps. According to band theory [32], there is a forbidden band ($E_{G1/2}$) between the conduction band (E_C) and valence band (E_V) of the semiconductor and insulator. Trap levels appear between the conduction band and valence band which are mainly derived from end groups, molecular chain breaks, branched chains, dielectric impurities, interfaces of different chemical clusters, amorphous interfaces of crystals and intermolecular chains of polymers etc.

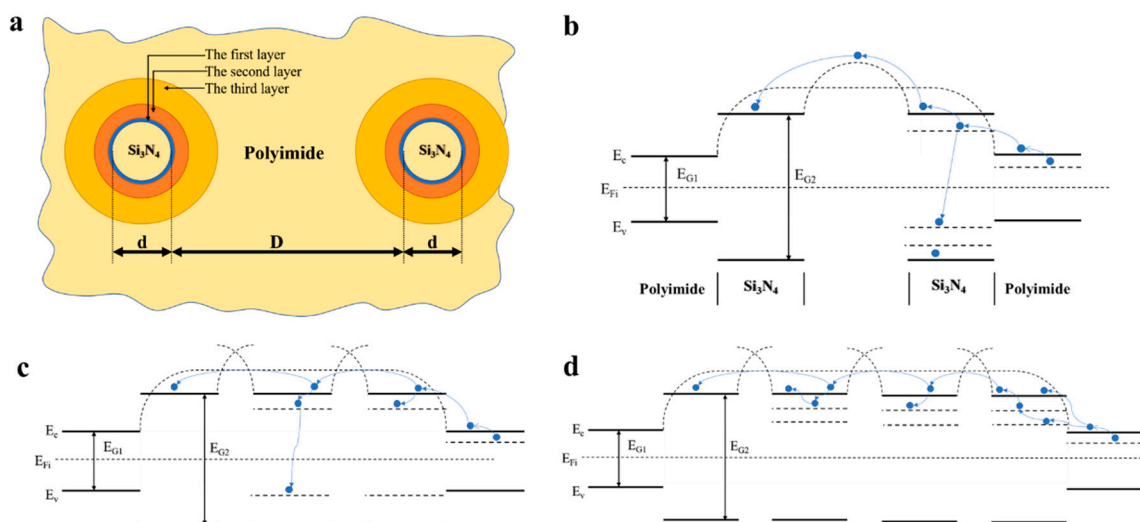


Figure 7. Schematic model of multi-core (a) and energy band structure for PI/Si₃N₄ composite films in different contents: 3 wt.% (b), 5 wt.% (c), 7 wt.% (d).

According to the literature [33], the bandgap of polyimide is around 2.9 eV and will decrease with the increasing of chain length. Meanwhile, the bandgap of Si₃N₄ is around 6.9 eV [34]. As shown in Figure 7b–d, there is a wide and high barrier between adjacent cells in pure polyimide. The potential barrier is higher when the silicon nitride nanoparticles contact the polyimide, due to its wide band

gap and small doping amount. Thus, charge carriers do not have enough energy to pass through the barrier, which makes it easy to be caught by deep traps and difficult to escape. If the doping ratio increases, the spacing between the particles will become smaller. The second and third layer is larger than the first layer, and the density of shallow traps is larger. Thus, the retention time of trapped charges is smaller, and the potential barrier is lower for mobile charge carriers. The energy obtained by charge carriers from the applied field would be increased. The polymer chain fracture may become easy, causing a lower breakdown field.

4. Conclusions

In summary, polyimide composites containing Si₃N₄ nanoparticles were successfully obtained by the in situ polymerization method. A 3 wt.% doped PI/Si₃N₄ film revealed an excellent dielectric performance (ϵ and $\tan\delta$ respectively from 3.3 to 3.2 and 0.0032 to 0.0112 at frequency range of 100 to 10⁶ Hz, and dielectric strength 237.42 MV/m). The space charge measurement results show that the accumulated charge density is almost negligible at the initial voltage in the PI/Si₃N₄-3% film. With the increasing of the doping amount, the initial accumulation of positive charge increases, completely suppressing the negative charge accumulation of the PI chain. The relationship between the breakdown strength and the space charge is based on the electronic transport in the nanoscale system, considering the large surface area of nanoparticles and the novel characteristics of the interface regions.

Author Contributions: Conceptualization, M.C. and W.Z.; Formal analysis, W.Z.; Funding acquisition, Q.C.; Investigation, W.Z.; Methodology, W.Z.; Project administration, M.C.; Resources, J.Z. and M.C.; Supervision, M.C.; Writing—original draft, W.Z.; Writing—review & editing, J.Z. and M.C. All authors have read and agreed to the published version of the manuscript.

Acknowledgments: The authors acknowledge financial support from Natural Science Foundation of China (51502063), Fundamental Research Fundation for Universities of Heilongjiang Province (LGYC2018JQ006), Project for Guiding Local Science and Technology Development by Central Government of China (ZY18C04), Harbin Funds for Distinguished Young Scientists (2017RAYXJ023) and Science Funds for Young Innovative Talents of HUST (201505).

Conflicts of Interest: The authors declare no conflict of interest.

References

1. Lee, C.J. Polyimidesiloxanes: Emerging materials for advanced packaging applications. *J. Electron. Mater.* **1989**, *18*, 313–318. [[CrossRef](#)]
2. Kreuz, J.A.A.; Edman, J.R.R. Polyimide films. *Adv. Mater.* **1998**, *10*, 1229–1232. [[CrossRef](#)]
3. Chen, M.H.; Yin, J.H.; Bu, W.B.; Liu, X.X.; Su, B.; Lei, Q.Q. Microstructure changes of polyimide/MMT-AlN composite hybrid films under corona aging. *Appl. Surf. Sci.* **2012**, *263*, 302–306. [[CrossRef](#)]
4. Ding, Y.; Hou, H.; Zhao, Y.; Zhu, Z.; Fong, H. Electrospun polyimide nanofibers and their applications. *Prog. Polym. Sci.* **2016**, *61*, 67–103. [[CrossRef](#)]
5. Dai, W.; Yu, J.; Liu, Z.; Wang, Y.; Song, Y.; Lyu, J.; Bai, H.; Nishimura, K.; Jiang, N. Enhanced thermal conductivity and retained electrical insulation for polyimide composites with SiC nanowires grown on graphene hybrid fillers. *Compos. Part A Appl. Sci. Manuf.* **2015**, *76*, 73–81. [[CrossRef](#)]
6. Fang, L.; Wu, W.; Huang, X.; He, J.; Jiang, P. Hydrangea-like zinc oxide superstructures for ferroelectric polymer composites with high thermal conductivity and high dielectric constant. *Compos. Sci. Technol.* **2015**, *107*, 67–74. [[CrossRef](#)]
7. Zhou, Y.; Wang, L.; Zhang, H.; Bai, Y.; Niu, Y.; Wang, H. Enhanced high thermal conductivity and low permittivity of polyimide based composites by core-shell Ag@SiO₂ nanoparticle fillers. *Appl. Phys. Lett.* **2012**, *101*, 012903. [[CrossRef](#)]
8. Liu, H.; Shen, Y.; Song, Y.; Nan, C.W.; Lin, Y.; Yang, X. Carbon nanotube array/polymer core/shell structured composites with high dielectric permittivity, low dielectric loss, and large energy density. *Adv. Mater.* **2011**, *23*, 5104–5108. [[CrossRef](#)]
9. Zhang, L.; Wang, W.; Wang, X.; Bass, P.; Cheng, Z.Y. Metal-polymer nanocomposites with high percolation threshold and high dielectric constant. *Appl. Phys. Lett.* **2013**, *103*, 232903. [[CrossRef](#)]

10. Liao, X.; Ye, W.; Chen, L.; Jiang, S.; Hou, H.; Jiang, S.; Wang, G.; Zhang, L. Flexible hdC-G reinforced polyimide composites with high dielectric permittivity. *Compos. Part A Appl. Sci. Manuf.* **2017**, *101*, 50–58. [[CrossRef](#)]
11. Lu, X.; Zhang, L.; Tong, Y.; Cheng, Z.Y. BST-P(VDF-CTFE) nanocomposite films with high dielectric constant, low dielectric loss, and high energy-storage density. *Compos. Part B Eng.* **2019**, *168*, 34–43. [[CrossRef](#)]
12. Luo, S.; Shen, Y.; Yu, S.; Wan, Y.; Liao, W.H.; Sun, R.; Wong, C.P. Construction of a 3D-BaTiO₃ network leading to significantly enhanced dielectric permittivity and energy storage density of polymer composites. *Energy Environ. Sci.* **2017**, *10*, 137–144. [[CrossRef](#)]
13. Hao, Y.; Wang, X.; Bi, K.; Zhang, J.; Huang, Y.; Wu, L.; Zhao, P.; Xu, K.; Lei, M.; Li, L. Significantly enhanced energy storage performance promoted by ultimate sized ferroelectric BaTiO₃ fillers in nanocomposite films. *Nano Energy* **2017**, *31*, 49–56. [[CrossRef](#)]
14. Li, D.; Li, B.; Yang, X.; Gao, S.; Zheng, Y. Fabrication and properties of in situ silicon nitride nanowires reinforced porous silicon nitride (SNNWs/SN) composites. *J. Eur. Ceram. Soc.* **2018**, *38*, 2671–2675. [[CrossRef](#)]
15. Diahm, S.; Pizzutilo, E.; Locatelli, M.-L. DC dielectric strength of epoxy/SiN₄ nanocomposites. In Proceedings of the 2016 IEEE International Conference on Dielectrics (ICD), Montpellier, France, 3–7 July 2016; Volume 1, pp. 72–75.
16. Xu, G.C.C.; Wang, J.; Ji, X.L.L.; Xiong, J.Y.Y.; Li, F. Effect of nano-silicon nitride on the mechanical and electric properties of polypropylene nanocomposite. *J. Compos. Mater.* **2007**, *41*, 2213–2223. [[CrossRef](#)]
17. He, H.; Fu, R.; Shen, Y.; Han, Y.; Song, X. Preparation and properties of Si₃N₄/PS composites used for electronic packaging. *Compos. Sci. Technol.* **2007**, *67*, 2493–2499. [[CrossRef](#)]
18. Yan, H.; Zhang, M.; Liu, C.; Zhang, J. Nano-Si₃N₄/epoxidized silane/cyanate ester composites for electronic packaging. *Polym. Bull.* **2013**, *70*, 2923–2933. [[CrossRef](#)]
19. Zhou, W.; Wang, C.; Ai, T.; Wu, K.; Zhao, F.; Gu, H. A novel fiber-reinforced polyethylene composite with added silicon nitride particles for enhanced thermal conductivity. *Compos. Part A Appl. Sci. Manuf.* **2009**, *40*, 830–836. [[CrossRef](#)]
20. Li, S.; Yin, G.; Bai, S.; Li, J. A new potential barrier model in epoxy resin nanodielectrics. *IEEE Trans. Dielectr. Electr. Insul.* **2011**, *18*, 1535–1543. [[CrossRef](#)]
21. Lian, R.; Lei, X.; Chen, Y.; Zhang, Q. Hyperbranched-polysiloxane-based hyperbranched polyimide films with low dielectric permittivity and high mechanical and thermal properties. *J. Appl. Polym. Sci.* **2019**, *136*, 1–8. [[CrossRef](#)]
22. Chen, M.; Qi, M.; Yao, L.; Su, B.; Yin, J. Effect of surface charged SiO₂ nanoparticles on the microstructure and properties of polyimide/SiO₂ nanocomposite films. *Surf. Coat. Technol.* **2017**, *320*, 59–64. [[CrossRef](#)]
23. Sun, W.L.; Gu, J.W.; Tian, L.D.; Yao, P.; Zhang, Q.Y. Synthesis and characterization of branched phenylethynyl-terminated polyimides. *J. Polym. Res.* **2015**, *22*, 85. [[CrossRef](#)]
24. Dong, S.; Hu, P.; Zhang, X.; Cheng, Y.; Fang, C.; Xu, J.; Chen, G. Facile synthesis of silicon nitride nanowires with flexible mechanical properties and with diameters controlled by flow rate. *Sci. Rep.* **2017**, *7*, 1–12. [[CrossRef](#)] [[PubMed](#)]
25. Farzana, R.; Rajarao, R.; Mansuri, I.; Sahajwalla, V. Sustainable synthesis of silicon nitride nanowires using waste carbon fibre reinforced polymer (CFRP). *J. Clean. Prod.* **2018**, *188*, 371–377. [[CrossRef](#)]
26. Wang, J.; Shi, Z.; Mao, F.; Chen, S.; Wang, X. Bilayer polymer metamaterials containing negative permittivity layer for new High-k materials. *ACS Appl. Mater. Interfaces* **2017**, *9*, 1793–1800. [[CrossRef](#)]
27. Chi, Q.; Gao, Z.; Zhang, C.; Cui, Y.; Dong, J.; Wang, X.; Lei, Q. Dielectric properties of sandwich-structured BaTiO₃/polyimide hybrid films. *J. Mater. Sci. Mater. Electron.* **2017**, *28*, 15142–15148. [[CrossRef](#)]
28. Donnay, M.; Tzavalas, S.; Logakis, E. Boron nitride filled epoxy with improved thermal conductivity and dielectric breakdown strength. *Compos. Sci. Technol.* **2015**, *110*, 152–158. [[CrossRef](#)]
29. Sun, Y.; Bealing, C.; Boggs, S.; Ramprasad, R. 50+ Years of Intrinsic Breakdown. *IEEE Electr. Insul. Mag.* **2013**, *29*, 8–15. [[CrossRef](#)]
30. McPherson, J.W. Determination of the nature of molecular bonding in silica from time-dependent dielectric breakdown data. *J. Appl. Phys.* **2004**, *95*, 8101–8109. [[CrossRef](#)]
31. Tanaka, T.; Kozako, M.; Fuse, N.; Ohki, Y. Proposal of a multi-core model for polymer nanocomposite dielectrics. *IEEE Trans. Dielectr. Electr. Insul.* **2005**, *12*, 669–681. [[CrossRef](#)]
32. Teyssedre, G.; Laurent, C. Charge transport modeling in insulating polymers: From molecular to macroscopic scale. *IEEE Trans. Dielectr. Electr. Insul.* **2005**, *12*, 857–874. [[CrossRef](#)]

33. Chu, S.; Wang, Y.; Wang, C.; Yang, J.; Zou, Z. Bandgap modulation of polyimide photocatalyst for optimum H₂ production activity under visible light irradiation. *Int. J. Hydrogen Energy* **2013**, *38*, 10768–10772. [[CrossRef](#)]
34. Ren, S.-Y.; Ching, W.Y. Electronic structures of β - and α -silicon nitride. *Phys. Rev. B* **1981**, *23*, 5454–5463. [[CrossRef](#)]



© 2020 by the authors. Licensee MDPI, Basel, Switzerland. This article is an open access article distributed under the terms and conditions of the Creative Commons Attribution (CC BY) license (<http://creativecommons.org/licenses/by/4.0/>).